Adsorption (2009) 15: 318–328
DOI 10.1007/s10450-009-9185-6

Effect of pore expansion and amine functionalization of mesoporous silica on CO_2 adsorption over a wide range of conditions

Youssef Belmabkhout · Abdelhamid Sayari

Published online: 17 April 2009

Abstract Adsorption of CO_2 was investigated over a wide range of conditions on a series of mesoporous silica adsorbents comprised of conventional MCM-41, pore-expanded MCM-41 silica (PE-MCM-41) and triamine surface-modified PE-MCM-41 (TRI-PE-MCM-41). The isosteric heat of adsorption, calculated from adsorption isotherms at different temperatures (298–328 K), showed a significant increase in CO_2–adsorbent interaction after amine functionnalization of PE-MCM-41, consistent with the high CO_2 uptake in the very low range of CO_2 concentration. The CO_2 adsorption isotherm and kinetics data showed the high potential of TRI-PE-MCM-41 material for CO_2 removal in gas purification and separation applications. With TRI-PE-MCM-41, the CO_2 selectivity over N_2 was drastically improved over a wide range of conditions compared to pure mesoporous silica. Moreover, the adsorption was reversible and fast, and the adsorbent was thermally stable and tolerant to moisture.

Keywords CO_2 adsorption · N_2 adsorption · Pore-expanded MCM-41 · Amine modified pore-expanded MCM-41 · CO_2 adsorption selectivity · CO_2 removal · Tolerance to moisture

Abbreviations

S_{BET}	Specific surface area m^2/g
V_p	Pore volume cm^3/g
D_p	Pore diameter nm
T	Temperature K
P	Pressure bar
m_{excess}	Excess adsorbed mass g/g
ρ_{gas}	Gas density g/cm^3
Ω	Reduced mass mmol/g
V_{ss}	Volume of the suspension system cm^3
$V_{adsorbent}$	Volume of the adsorbent cm^3
q_{st}	Isosteric heat kJ/mol
k	Kinetics rate constant s^{-1}

Y. Belmabkhout · A. Sayari (✉)
Department of Chemistry and Department of Chemical Engineering, University of Ottawa, Ottawa, Ontario, K1N 6N5, Canada
e-mail: abdel.sayari@uottawa.ca

1 Introduction

Carbon Dioxide (CO_2) is a major greenhouse gas with significant contribution to global warming (Halmann and Stenberg 1999). Removal of CO_2 from different gas streams is becoming increasingly important for various applications like power generation, natural gas, stack gas and hydrogen purification as well as closed-circuit breathing systems for use in confined spaces such as manned space shuttles (Satyapal et al. 2001), and in emergency situations. The recovered CO_2, with different degrees of purity, has also numerous applications in the chemical industry.

To decrease the CO_2 impact on climate change and to increase the CO_2 concentration in the recovered effluents, more efficient CO_2 removal technologies are needed. Liquid phase absorption in amine solutions has been widely used to treat gases with medium to high CO_2 concentration, but due to the high regeneration cost of the absorbent and corrosion problems (Veawab et al. 1999), it is highly desirable to develop less energy intensive technologies like adsorption (Ruthven et al. 1994) and membrane separation (Hong et al. 2008). It is widely recognized that adsorption is a promising technology provided that materials with high selectivity toward CO_2 are available (Aaron

and Tsouris 2005). During the recent years, intensive research activity has been focused on the development of technologies based on sorption of CO_2 on oxide surfaces (Wang et al. 2008) at high temperature, as well as adsorption using zeolites (Goj et al. 2002; Cavenati et al. 2004; Akten et al. 2003; Belmabkhout et al. 2007), carbon (Himeno et al. 2005) and metal-organic frameworks (MOFs) (Millward and Yaghi 2005; Bourrelly et al. 2005; Yang et al. 2008). The discovery of periodic mesoporous materials like MCM-41 silica has resulted in extensive research activity in their synthesis and applications, particularly for separation and catalysis (Sayari 1996, Sayari and Jaroniec 2008). Although, the use of organically-modified silica materials for CO_2 removal was extensively studied using different mesoporous silica supports such as MCM-41, SBA-15, MCM-48 and PE-MCM-41 (for a review see Harlick and Sayari 2007 and reference therein); adsorption of CO_2 was investigated in a limited range of CO_2 concentration, temperature and pressure.

In a previous contribution (Harlick and Sayari 2007), our group showed that the triamine-modified PE-MCM-41 (TRI-PE-MCM-41) adsorbent obtained by post-synthesis pore expansion of MCM-41 and its surface functionalization, showed promising properties in terms of CO_2 uptake and rate of adsorption for 5% CO_2 in N_2 at room temperature. In the current work, we investigated the adsorption of CO_2 over a wide range of pressure up to 20 bar and at different temperatures (298, 308, 318, 328 K) for the parent MCM-41 mesoporous silica, the post-synthesis pore-expanded MCM-41 (PE-MCM-41) and its triamine-modified counterpart (TRI-PE-MCM-41). This work showed how CO_2 adsorption properties evolve from pure mesoporous silica to structurally or organically modified materials over a wide range of CO_2 pressure and at different temperatures. Upon amine functionalization, the CO_2 uptake was remarkably improved, particularly, at low CO_2 concentration and the material was capable of both chemical and physical adsorption at low pressure and high pressure, respectively. Using CO_2-N_2 mixture for illustration, it was found that surface functionalization strongly affects the selectivity toward CO_2. Moreover, the organically-modified material was found to be stable and recyclable up to 423 K.

2 Experimental

2.1 Materials

Figure 1 shows the procedure for the synthesis of MCM-41 and post-synthesis hydrothermal pore-expansion (Sayari et al. 1998). MCM-41 silica was prepared in the presence of cetyltrimethylammonium bromide (CTAB) at 353 K (Sayari

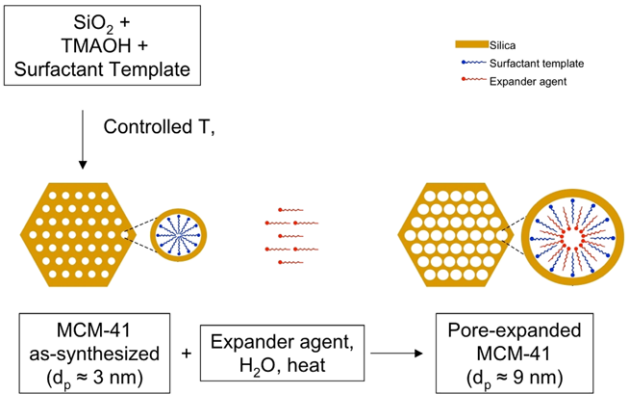

Fig. 1 Synthesis of MCM-41 and post-synthesis pore expansion

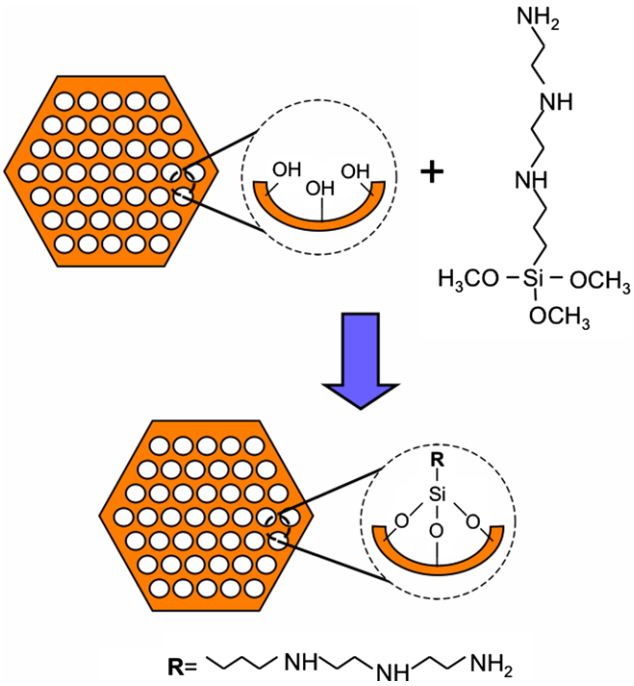

Fig. 2 Functionalization of mesoporous (PE-MCM-41) silica by grafting

and Yang 2000). The expander agent used for the preparation of PE-MCM-41 was dimethyldecylamine (DMDA). More details about the procedure may be found elsewhere (Franchi et al. 2005; Harlick and Sayari 2007). Under appropriate conditions, i.e., DMDA/MCM-41 ratio, temperature and time of the post-synthesis hydrothermal stage, the pore size of MCM-41 can be expanded from ca. 3.5 nm up to ca. 20 nm. As shown earlier (Harlick and Sayari 2007), the pore enlargement is critical for improved incorporation of organic functionalities onto the internal surface of the material and for its CO_2 adsorptive properties.

Figure 2 shows a schematic diagram of the amine functionalization. The PE-MCM-41 was used as a support for post-synthesis grafting of 3-[2-(2-aminoethylamino)ethyl-

amino] propyltrimethoxysilane (TRI). Because of its wide open structure and its enlarged pores, PE-MCM-4 was able to accommodate a high loading of amine groups. More details about the procedure may be found elsewhere (Harlick and Sayari 2007).

Carbon dioxide (99.99%), nitrogen (99.999%), 1 and 10% carbon dioxide in nitrogen, 0.1% carbon dioxide in helium and pure helium (99.999%) were provided by BOC Canada.

2.2 Material characterization

Nitrogen adsorption measurements were performed at 77 K using a Micromeritics ASAP 2020 automated volumetric instrument. Prior to each analysis, the materials were degassed at 423 K under high vacuum (1.3×10^{-5} mbar). The specific surface area (S_{BET}) was determined using the BET method in 0.05–0.2 relative pressure range and the pore size distribution (PSD) was calculated using the KJS (Kruk, Jaroniec, Sayari) approach (Kruk et al. 1997). The pore diameter (D_p) corresponds to the maximum of the PSD and the total pore volume was calculated from the amount adsorbed at a relative pressure of about 0.99.

2.3 Adsorption and kinetics measurements

Adsorption equilibrium and kinetics measurements of pure CO_2 were performed using a Rubotherm gravimetric-densimetric apparatus (Rubotherm Germany), schematically represented in Fig. 3 and composed mainly of a magnetic suspension balance (MSB) and a network of valves, flowmeters and temperature and pressure sensors. It operates both in closed and open loops.

The MSB overcomes the disadvantages of other traditional microbalances by separating the sensitive microbalance from the sample and the measuring atmosphere (Dreisbach et al. 2003). In a typical adsorption experiment, the adsorbent was weighed and placed in a basket suspended by a permanent magnet through an electromagnet. The cell in which the basket is housed was then closed, and vacuum or high pressure was applied. This system is able to perform adsorption measurements in a wide range of gas pressure from 0 to 6 MPa. The adsorption temperature may also be controlled within the range of 298 to 423 K. The clean (outgassed) adsorbent was exposed to flowing gas at constant temperature. The change in the weight of the adsorbent sample as well as the pressure and temperature were measured continuously until the thermodynamic equilibrium was reached. In a typical kinetic experiment, the gas was introduced in such a way to reach the desired pressure in 5–10 s. The flow rate was 100 ml/min. The change in the weight of the adsorbent sample as well as the pressure and temperature were measured continuously until the thermodynamic equilibrium was reached. The gravimetric method allows the direct measurement of the reduced mass Ω.

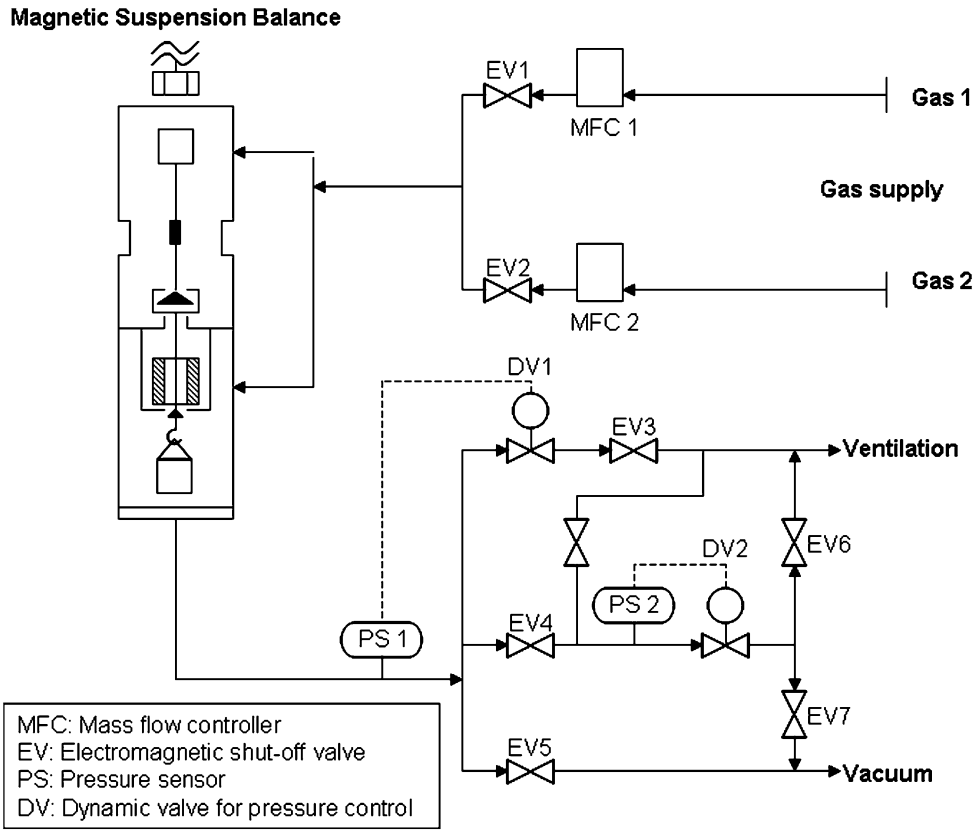

Fig. 3 Schematic diagram of the Rubotherm gravimetric-densimetric set-up

Correction for the buoyancy effect is required to determine the excess adsorbed amount (Belmabkhout et al. 2004; Dreisbach et al. 2003) using (1), where $V_{adsorbent}$ and V_{ss} refer to the volume of the adsorbent and the volume of the suspension system, respectively. These volumes were determined using the helium isotherm method by assuming that helium penetrates in all the open pores of the materials without being adsorbed (Sircar 2002; Belmabkhout et al. 2004). The density of the gas was determined experimentally using a volume-calibrated titanium cylinder. By weighing this calibrated volume in the gas atmosphere, the local density of the gas was also determined. Simultaneous measurement of gas uptake and gas phase density as a function of pressure and temperature was thus possible.

$$\Omega = m_{excess} - \rho_{gas}(V_{adsorbent} + V_{ss}) \quad (1)$$

The pressure was measured using two Drucks high pressure transmitters ranging from 0.5 to 18 bar and 1 bar to 80 bar, respectively, and one MKS low pressure transmitter ranging from 0 to 1 bar. Prior to each adsorption experiment, about 0.5 to 1 g sample was outgassed up to 423 K and a residual pressure 10^{-4} mbar. The temperature during adsorption measurements was held constant using a thermostated circulating fluid.

3 Results and discussion

3.1 Material characterization

Figure 4 and Table 1 show the structural characteristics of the MCM-41, PE-MCM-41 and TRI-PE-MCM-41 materials. All the nitrogen adsorption isotherms corresponded to type IV according to the IUPAC classification, which is characteristic of mesoporous materials. Although it had broader PSD, PE-MCM-41 had significantly larger pore size and volume than MCM-41 and exhibited comparably high surface area. The difference between PE-MCM-41 and TRI-PE-MCM-41 in terms of pore diameter was attributed to the space occupied by the amine-containing organic species on the surface.

3.2 Adsorption measurements of pure CO_2

Figure 5 shows the adsorption isotherms for MCM-41, PE-MCM-41 and TRI-PE-MCM-41 materials at 298 K and up

Table 1 Structural properties of materials

Materials	S_{BET} (m^2/g)	V_p (cm^3/g)	D_p (nm)
MCM-41	1490	0.99	3.3
PE-MCM-41	1230	3.09	11.7
TRI-PE-MCM-41	367	0.87	9.4

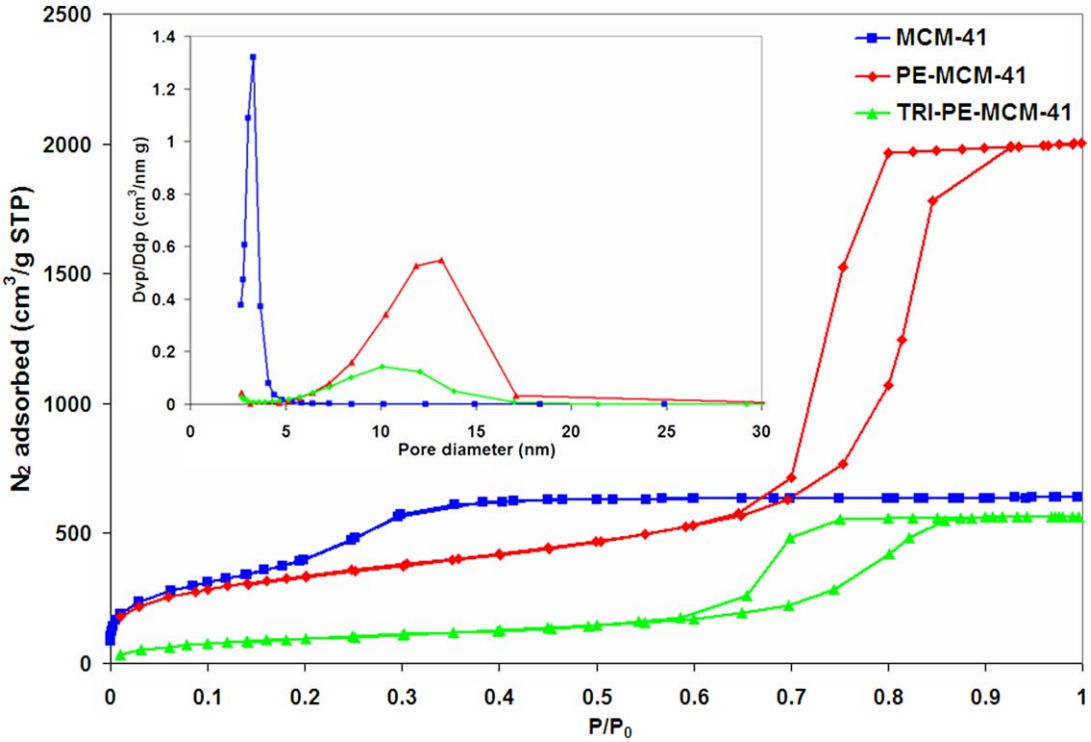

Fig. 4 N_2 adsorption isotherms for materials; *inset* represents the pore size distributions

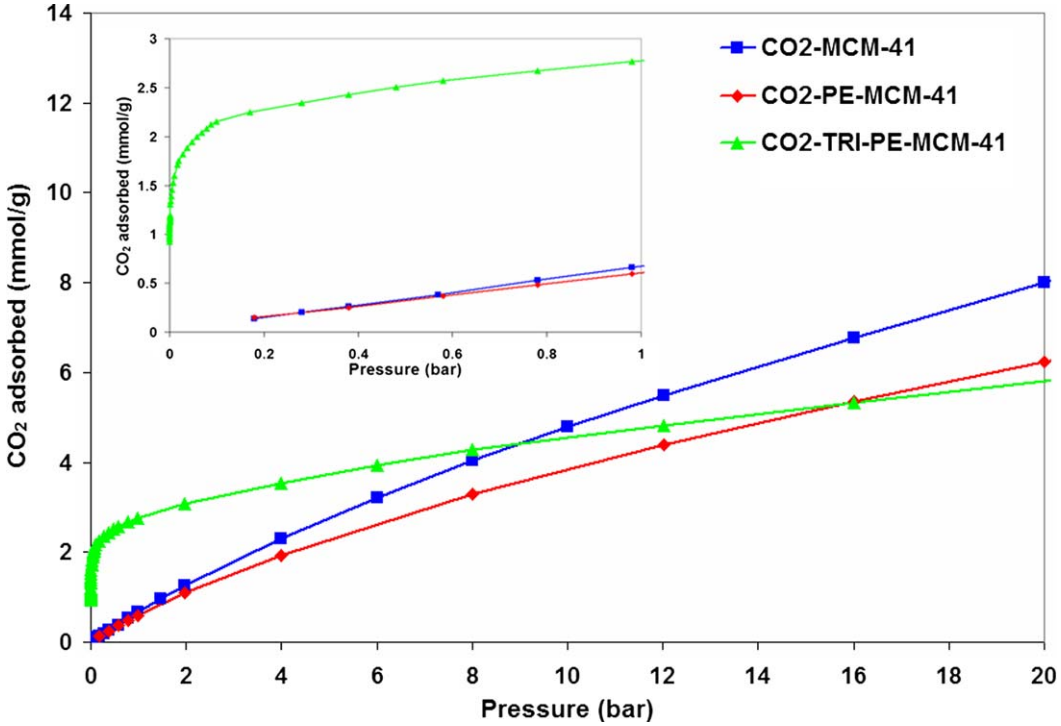

Fig. 5 Gravimetric CO_2 adsorption uptake versus pressure for materials at 298 K; *inset* showing the results at low pressure

to 20 bar. The reproducibility of data was very good. The average errors calculated were 1–2% and 2–5% for CO_2 and N_2 adsorption at 298 K, respectively. These values increase slightly at higher the temperature of adsorption, as they depend strongly on the total excess adsorption uptake. Because the very low N_2 uptake on TRI-PE-MCM-41, the uncertainty may exceed 50%. TRI-PE-MCM-41 exhibited significant CO_2 uptake in the low CO_2 concentration range, due mainly to the strong interaction of CO_2 with the surface amine sites. The adsorption uptake at 5% of dry CO_2 was 2.05 mmol/g (9.02 wt%) while at the same concentration, CO_2 adsorption on MCM-41 and PE-MCM-41 was very small.

The sequence in terms of CO_2 uptake at low pressure of CO_2 was TRI-PE-MCM-41 $\gg$ PE-MCM-41 $\approx$ MCM-41. At moderate and high pressures, the slope of TRI-PE-MCM-41 adsorption isotherm decreased steeply in comparison to MCM-41 and PE-MCM-41 materials indicative of the decrease of CO_2–adsorbent interactions. Nevertheless, the CO_2 uptake continued to increase with increasing CO_2 pressure. The sequence in terms of CO_2 uptake at high pressure (e.g., 20 bar) was MCM-41 > PE-MCM-41 > TRI-PE-MCM-41, in good agreement with the sequence in terms of BET surface area. In fact, at low CO_2 concentration, the adsorption on TRI-PE-MCM-41 was chemical in nature while physical adsorption within the pores occurred at high pressure. Thus, TRI-PE-MCM-41 combined both chemical and physical adsorption.

3.3 CO_2 isosteric heat of adsorption

Figure 6 shows the evolution of the isosteric heat of adsorption as a function of CO_2 loading for MCM-41, PE-MCM-41 and TRI-PE-MCM-41 materials.

The isosteric heat (q_{st}) of adsorption is a sensitive probe for adsorption non-uniformity (heterogeneity) and hence for surface structure, reflecting in turn the distribution of surface energy of the adsorbent. The q_{st} of CO_2 adsorption on MCM-41, PE-MCM-41 and TRI-PE-MCM-41 were calculated from adsorption isotherms at different temperatures (298, 308, 318, 328 K). As shown in Figs. 7, 8 and 9. MCM-41 had almost constant q_{st} vs. CO_2 loading, reflecting the uniform nature of the surface and the values determined at low loading (ca. 22 kJ/mol) are comparable to typical values for MCM-41 silica (Yufeng and Seaton 2006). After pore expansion, the CO_2 q_{st} decreased slightly as a function of loading indicative of the surface heterogeneity of PE-MCM-41, in good agreement with its broader PSD. After functionalization the q_{st} was significantly enhanced due to chemical interactions with amine sites at low loading. As the CO_2 loading over TRI-PE-MCM-41 increased, the CO_2 q_{st} decreased significantly, reflecting the high degree of heterogeneity of the surface energy. Two different slopes were clearly observed, before and after 2.5 mmol/g

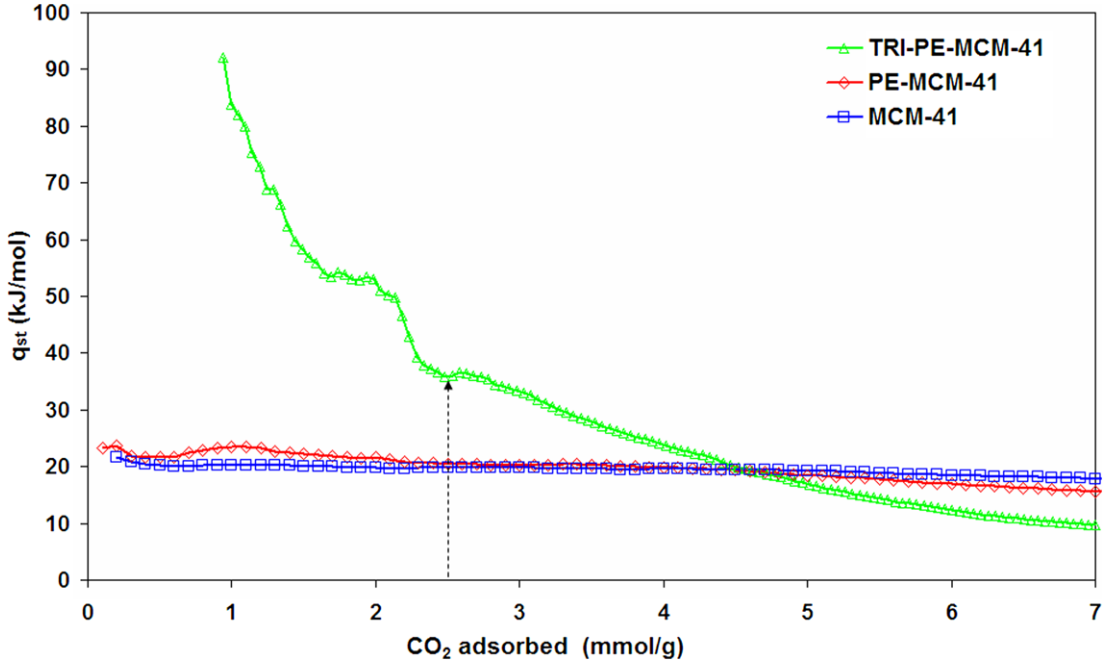

Fig. 6 Isosteric heat of adsorption of CO_2 vs. loading for MCM-41, PE-MCM-41 and TRI-PE-MCM-41

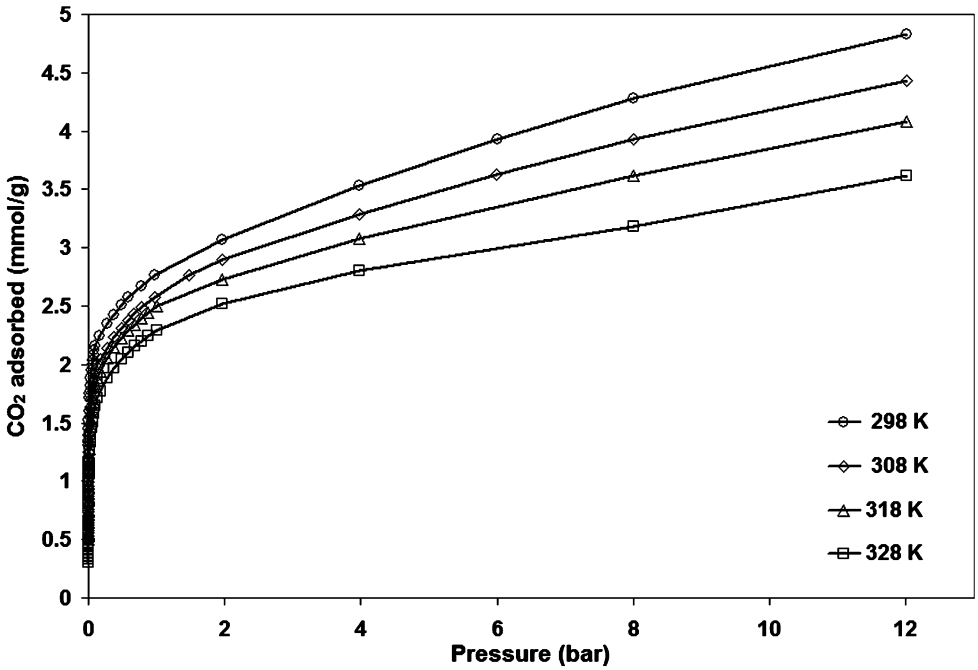

Fig. 7 CO_2 adsorption isotherms for TRI-PE-MCM-41

CO_2 uptake (as indicated by the arrow in Fig. 6) indicative of the occurrence of both chemical and physical adsorption mechanisms. Generally the error on the isosteric heat varies between 5% to 20% depending on the temperature range and the loading (the error is larger at low loading). The sequence of the q_{st} at low loading was TRI-PE-MCM-41 $\gg$ PE-MCM-41 $\approx$ MCM-41 consistent with the sequence of the CO_2 adsorption uptake at low loading.

3.4 Kinetics of CO_2 adsorption

Figure 10 shows the kinetic curve of adsorption at 298 K and 1 bar for MCM-41, PE-MCM-41 and TRI-PE-MCM-41 materials determined using pure CO_2 flowing at 100 mL/min.

The CO_2 adsorption kinetic curves were fitted to Linear Driving Model (LDF) (Murcia et al. 2003), to estimate the

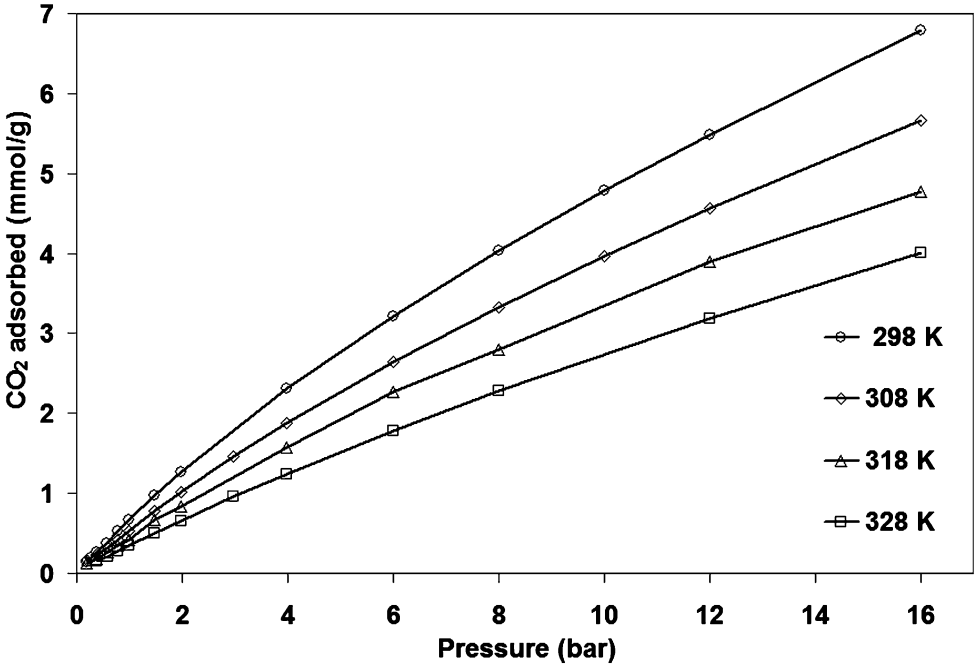

Fig. 8 CO_2 adsorption isotherms for MCM-41

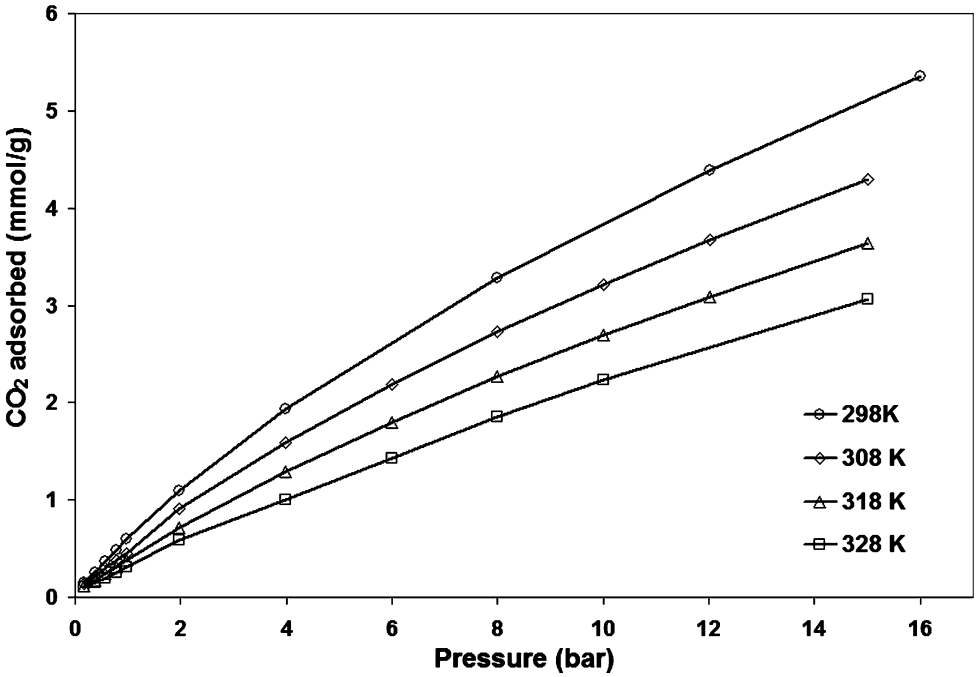

Fig. 9 CO_2 adsorption isotherms for PE-MCM-41

kinetic rate constant of CO_2 adsorption. The LDF model is described by (2):

$$\frac{n_t}{n_e} = 1 - e^{-kt} \tag{2}$$

where n_e is the equilibrium uptake at 298 K and 1 bar, n_t is the uptake at time t and k is the kinetic rate constant. The results of the fit are shown in Fig. 11 and Table 2. The CO_2 kinetic rate constant was significantly higher upon pore expansion, most likely due to the larger pores and higher pore volume of PE-MCM-41 in comparison to MCM-41. The TRI-PE-MCM-41 seems to have higher kinetic rate constant than PE-MCM-41 and MCM-41, up to 0.5 fractional uptake n_t/n_e. The sequence in terms of LDF kinetic rate constant was TRI-PE-MCM-41 > PE-MCM-41 > MCM-41. At higher fractional uptake, the fit for TRI-PE-MCM-41 was no longer satisfactory and the kinetic rate constant seemed to decrease to ca. 2×10^{-3} s^{-1}. This may be associated with mass transfer barriers caused by the

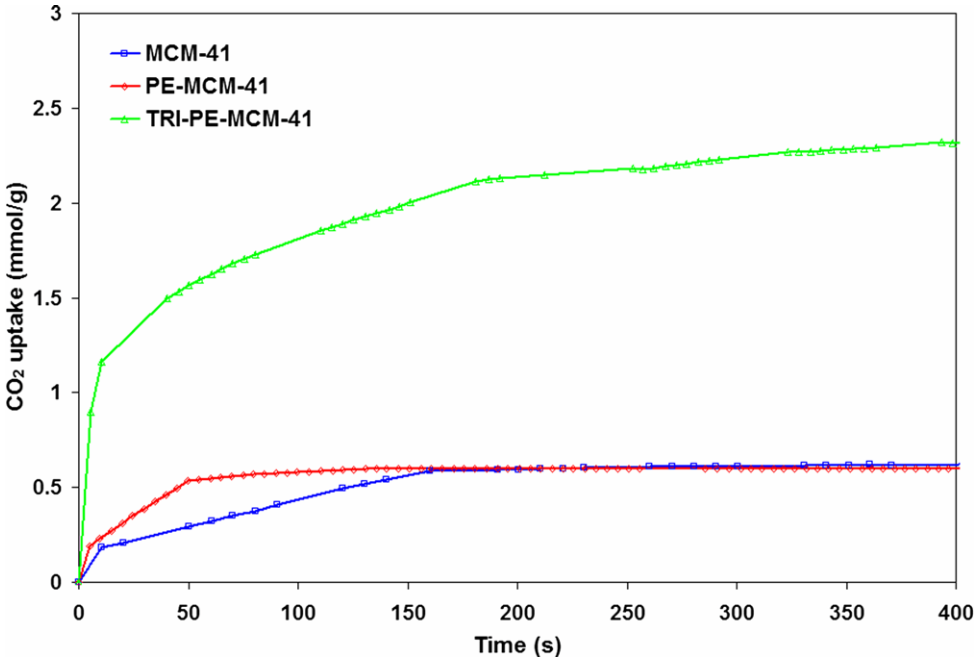

Fig. 10 Kinetics of CO_2 adsorption at 1 bar and 298 K for MCM-41, PE-MCM-41 and TRI-PE-MCM-41

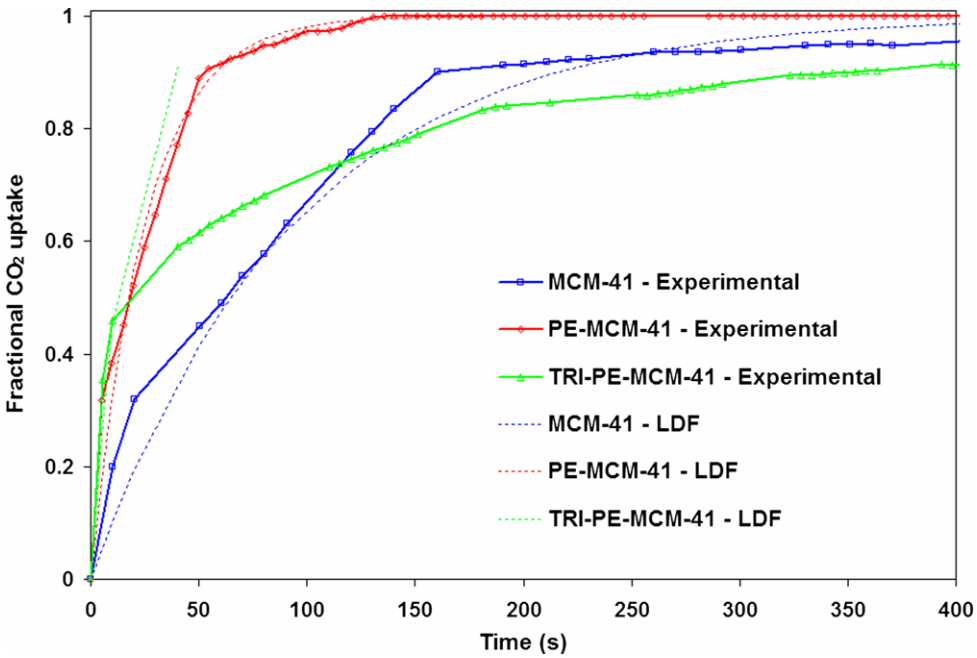

Fig. 11 Fractional CO_2 uptake (n_t/n_e) at 1 bar and 298 K for MCM-41, PE-MCM-41 and TRI-PE-MCM-41

Table 2 LDF kinetic rate constant of CO_2 adsorption

Materials	k (LDF kinetic rate)/s^{-1}
MCM-41	1.07×10^{-2}
PE-MCM-41	4×10^{-2}
TRI-PE-MCM-41	6×10^{-2} (up to 0.5)

occurrence of both chemical and physical adsorption and by the presence of amine—containing species on the pore walls.

3.5 Selectivity of adsorption of CO_2 over N_2

Figure 12 shows the CO_2 and N_2 adsorption isotherms up to 20 bar for MCM-41, PE-MCM-41 and TRI-PE-MCM-41 materials at ambient temperature. The nitrogen adsorption capacity on TRI-PE-MCM-41 was very small in comparison to CO_2 uptake in the whole range of pressure.

Figure 13 shows the evolution of the CO_2/N_2 molar selectivity ratio, i.e, the ratio of both pure CO_2 and N_2 adsorbed in separate experiments, as a function of pressure for MCM-41, PE-MCM-41 and TRI-PE-MCM-41 materials. At

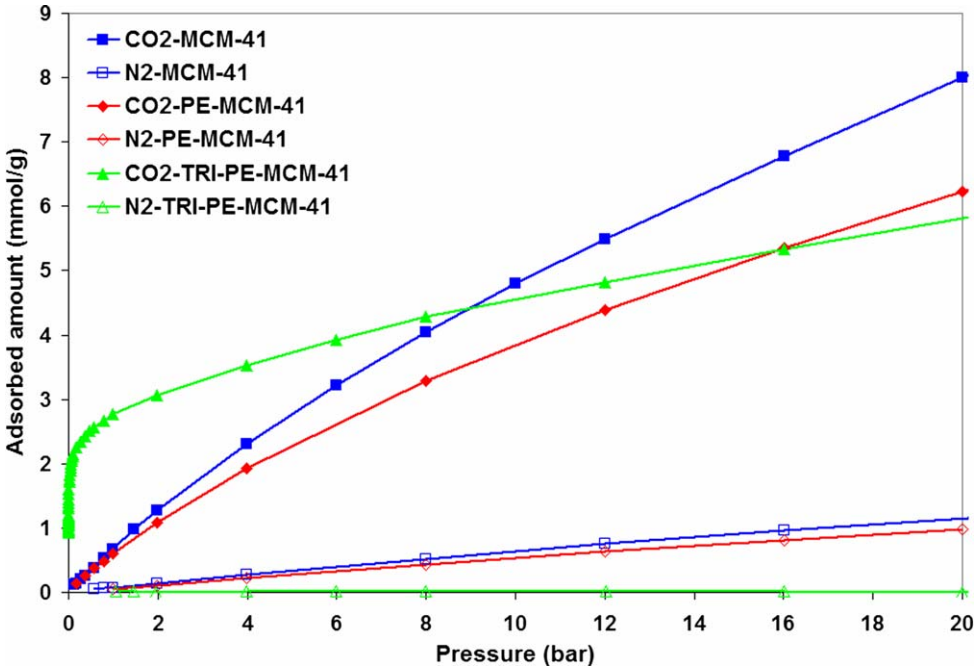

Fig. 12 CO_2 and N_2 adsorption isotherms for MCM-41, PE-MCM-41 and TRI-PE-MCM-41 at 298 K

Table 3 CO_2/N_2 molar selectivity ratio for materials at 1 bar and 298 K and the corresponding selectivity calculated using IAST

Materials	CO_2/N_2 molar selectivity ratio	IAST CO_2 vs. N_2 selectivity for CO_2:N_2 = 20:80
MCM-41	9	11
PE-MCM-41	9	12
TRI-PE-MCM-41	308	IAST not applicable

Table 4 Equilibrium capacity of CO_2 adsorption in the presence of 27% relative humidity at different CO_2 concentrations

Gas composition	Equilibrium capacity/mmol/g	
	Dry feed	Humid feed (27% RH)
1000 ppm CO_2 in He	1.2 (5.28 wt%)	1.43 (6.3 wt%)
5% CO_2 in N_2	2.05 (9.02 wt%)	2.25 (9.9 wt%)

$P = 1$ bar and $T = 298$ K, the CO_2/N_2 molar ratio selectivity over MCM-41 and PE-MCM-41 was 9. However, the selectivity predicted by the Ideal Adsorption Solution Theory (IAST) (Myers and Prausnitz 1965), which takes into account the competition between both adsorbates was found to be slightly higher (ca. 11). The IAST does not apply for chemical adsorbents like TRI-PE-MCM-41.

As shown in Fig. 13 and Table 3, the CO_2/N_2 molar selectivity ratio after surface functionalization was drastically improved over the whole range of pressure, indicative of the high selectivity of CO_2 adsorption over N_2 for the TRI-PE-MCM-41. Under the same conditions (1 bar CO_2, 298 K), the CO_2/N_2 molar ratios for 13X zeolite and activated carbon were reported to be 18 and 8, respectively (Siriwardane et al. 2001).

3.6 Thermal stability and cyclability for TRI-PE-MCM-41

For practical applications, the adsorbent should not only possess a high adsorption capacity for CO_2, and high selectivity over other species but also display a stable cyclic adsorption–desorption performance during prolonged operation. Figure 14 illustrates the adsorptive capacity of the TRI-PE-MCM-41 material during repetitive cycles of CO_2 adsorption at 298 K using CO_2:N_2 = 5:95 mixture and desorption under flowing N_2 at 473 K. Examination of the cyclical data reveals that the performance of the TRI-PE-MCM-41 adsorbent is fairly stable, with only minor decrease in the adsorption capacity (0.03 mmol/g of CO_2, i.e., 1.5% of initial capacity) after seven adsorption–desorption cycles. The loss of performance may be mitigated by regenerating the material at lower temperature, e.g., 353 K.

3.7 Tolerance to moisture

The separation and removal of CO_2 often involve gaseous feed streams containing varying amounts of water vapor. Table 4 shows the equilibrium capacity at 27% relative humidity (RH) for CO_2 at different concentrations. The adsorption experiments were performed by first adsorbing water vapor, i.e., by passing pure N_2 through a temperature controlled H_2O saturator, until equilibrium and then switching to CO_2:N_2 = 5:95 passing through the same H_2O satura-

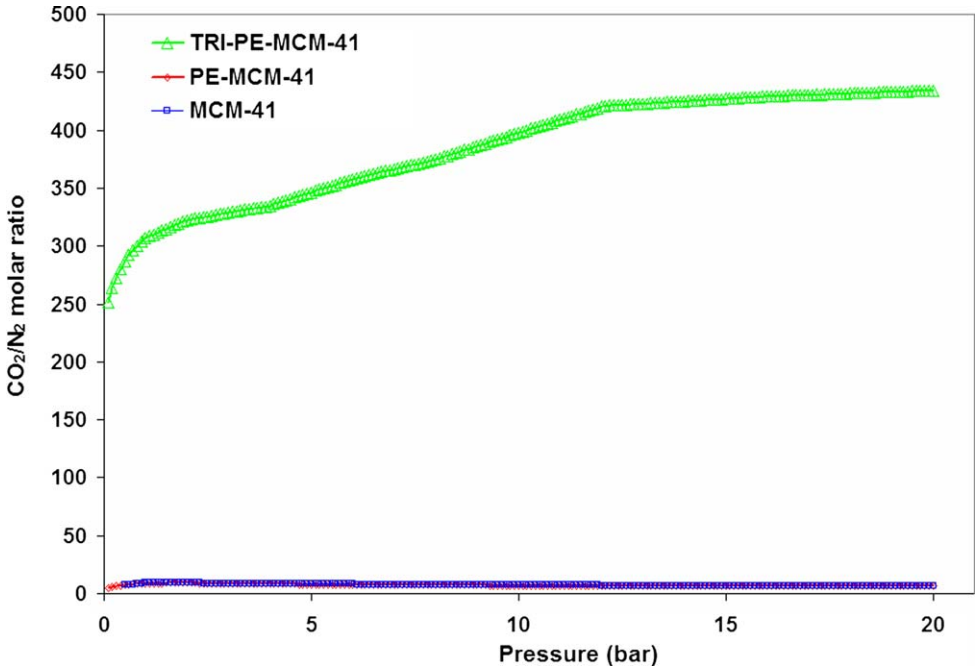

Fig. 13 CO_2/N_2 adsorption molar ratio vs pressure for MCM-41, PE-MCM-41 and TRI-PE-MCM-41 at 298 K

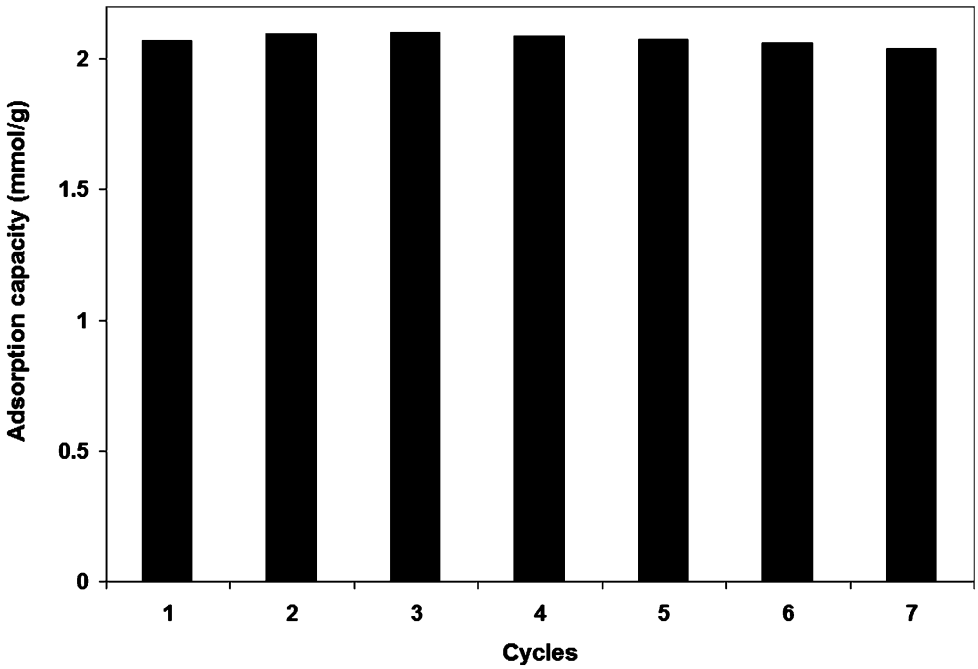

Fig. 14 Cyclical adsorption over TRI-PE-MCM-41:adsorption CO_2:N_2 = 5:95 at 298; desorption at 423 K under nitrogen

tor. In contrast to other CO_2 adsorbents like zeolites (Brandani and Ruthven 2004), the equilibrium CO_2 adsorption capacity of TRI-PE-MCM-41 in the presence of humidity was improved in comparison to adsorption of dry CO_2. At 27% RH, 19% and 10% gain was observed for 0.1% and 5% CO_2 concentration, respectively. Knowing that adsorption of N_2 is very small in both dry and humid conditions, we can conclude clearly that the selectivity of CO_2 over N_2 in the presence of water vapor will be as high as in dry gaseous streams.

4 Conclusion

Adsorption of CO_2 on a series of mesoporous pure silica such as MCM-41, PE-MCM-41 and amine-functionalized TRI-PE-MCM-41 was investigated over a wide range of pressure at different temperatures. Compared to MCM-41, the TRI-PE-MCM-41 adsorbent exhibited considerably larger CO_2 adsorption capacity, particularly at low to moderate pressure. Moreover, TRI-PE-MCM-41 exhibited much higher CO_2/N_2 molar selectivity ratio than MCM-41 and

PE-MCM-41. TRI-PE-MCM-41 was also completely reversible CO_2 adsorbent, recyclable and thermally stable at 423 K. While MCM-41 and PE-MCM-41 were purely physical adsorbents characterized by weak and relatively constant CO_2–adsorbent interactions (ca. 25–20 kJ/mol), the TRI-PE-MCM-41 showed decreasing CO_2–adsorbent interactions due to the effect of chemical adsorption and the transition to physisorption. At low CO_2 concentration, chemical adsorption with high isosteric heat (ca. 90 kJ/mol) was dominant, whereas at higher pressure, physical adsorption with weaker CO_2–adsorbent interactions prevailed. In contrast to zeolites, the TRI-PE-MCM-41 CO_2 uptake increased in the presence of humidity. This is a desirable property for potential applications in gas purification and separation.

Acknowledgements We thank the Natural Science and Engineering Council of Canada (NSERC) for financial support. A.S. is the Government of Canada Research Chair in Nanostructured Materials for Catalysis and Separation (2001–2015).

References

Aaron, D., Tsouris, C.: Separation of CO_2 from flue gas: a review. Sep. Sci. Technol. **40**, 321–348 (2005)

Akten, E.D., Siriwardane, R., Sholl, D.S.: Monte Carlo simulation of single-and binary-component adsorption of CO_2, N_2 and H_2 in zeolite Na-4A. Energy Fuels **17**, 977–983 (2003)

Belmabkhout, Y., Frère, M., De Weireld, G.: High-pressure adsorption measurements. A comparative study of the volumetric and gravimetric methods. Meas. Sci. Technol. **15**, 848 (2004)

Belmabkhout, Y., Pirngruber, G., Jolimaitre, E., Methivier, A.: A complete experimental approach of synthesis gas separation studies using static gravimetric and dynamic inverse chromatographic methods. Adsorption **13**, 341–349 (2007)

Bourrelly, S., Llewellyn, P.L., Serre, C., Millange, F., Loiseau, T., Férey, G.: Different adsorption behaviors of methane and carbon dioxide in the isotypic nanoporous metal terephthalates MIL-53 and MIL-47. J. Am. Chem. Soc. **127**, 13519–13521 (2005)

Brandani, F., Ruthven, D.: The effect of water on the adsorption of CO_2 and C_3H_8 on type X zeolites. Ind. Eng. Chem. Res. **43**, 8339–8344 (2004)

Cavenati, S., Grande, C.A., Rodrigues, A.E.: Adsorption equilibrium of methane, carbon dioxide, and nitrogen on zeolites 13X at high pressures. J. Chem. Eng. Data **49**, 1095–1101 (2004)

Dreisbach, F., Seif, R., Losch, H.W.: Adsorption equilibria of CO/H_2 with a magnetic suspension balance. Purely gravimetric measurements. J. Therm. Anal. Calorim. **71**, 73–82 (2003)

Franchi, R.S., Harlick, P.J.E., Sayari, A.: Application of pore-expanded mesoporous silica. 2. Development of a high-capacity, water tolerant adsorbent for CO_2. Ind. Eng. Chem. Res. **44**, 8007–8013 (2005)

Goj, A., Sholl, D.S., Akten, E.D., Kohen, D.: Atomistic simulations of CO_2 and N_2 adsorption in silica zeolites: the impact of size and shape. J. Phys. Chem. B **106**, 8367–8375 (2002)

Halmann, M.M., Stenberg, M.: Greenhouse Gas Carbon Dioxide Mitigation. CRC Press LLC, Boca Raton (1999)

Harlick, P.J.-E., Sayari, A.: Application of pore-expanded mesoporous silica 5. Triamine grafted material with exceptional CO_2 dynamic and equilibrium adsorption performance. Ind. Eng. Chem. Res. **46**, 446–458 (2007)

Himeno, S., Komatsu, T., Fujita, S.: High-pressure adsorption equilibria of methane and carbon dioxide on several activated carbons. J. Chem. Eng. Data **50**, 369–376 (2005)

Hong, M., Li, S., Falconer, J.L., Noble, R.D.: Hydrogen purification using a SAPO-34 membrane. J. Membr. Sci. **307**, 277–283 (2008)

Kruk, M., Jaroniec, M., Sayari, A.: Application of large pore MCM-41 molecular sieve to improve pore size analysis using nitrogen adsorption measurements. Langmuir **13**, 6227–6273 (1997)

Millward, A.R., Yaghi, O.M.: Metal-organic frameworks with exceptionally high capacity for storage of carbon dioxide at room temperature. J. Am. Chem. Soc. **127**, 17998–17999 (2005)

Murcia, A.B., Fletcher, A.J., Garcia-Martinez, J., Cazorla-Amoros, D., Linares-Solano, A., Thomas, K.M.: Probe molecule kinetics studies of adsorption on MCM-41. J. Phys. Chem. B **107**, 1012–1020 (2003)

Myers, A.L., Prausnitz, J.M.: Thermodynamics of mixed gas adsorption. AIChE J. **11**, 121–127 (1965)

Ruthven, D.M., Farooq, S., Knaebal, K.S.: Pressure Swing Adsorption. VCH, New York (1994)

Satyapal, S., Filburn, T., Trela, J., Strange, J.: Performances and properties of a solid amine sorbent for carbon dioxide removal in space life support application. Energy Fuels **15**, 250–255 (2001)

Sayari, A.: Catalysis by crystalline mesoporous molecular sieves. Chem. Mater. **8**, 1840–1852 (1996)

Sayari, A., Jaroniec, M.: Nanoporous Materials. World Scientific Publ., Singapore (2008)

Sayari, A., Yang, Y.: Highly ordered MCM-41 silica prepared in the presence of decyltrimethlammomium bromide. J. Phys. Chem. B **104**, 4835–4839 (2000)

Sayari, A., Kruk, M., Jaroniec, M., Moudrakovski, I.L.: New approaches to pore size engineering of mesoporous silicates. Adv. Mater. **10**, 1376–1379 (1998)

Sircar, S.: Role of helium void measurement in estimation of Gibbsian surface excess. In: Kaneko, K. (ed.) Proceedings of Fundamental of Adsorption 7, pp. 656–663. IK International, Chiba City (2002)

Siriwardane, R.V., Shen, M.S., Fisher, E.P., Poston, J.A.: Adsorption of CO_2 on molecular sieves and activated carbon. Energy Fuels **15**, 279–284 (2001)

Veawab, A., Tontiwachwuthikul, P., Chakma, A.: Corrosion behaviour of carbon dioxide steel in the CO_2 absorption process using aqueous amine solutions. Ind. Eng. Chem. Res. **38**, 3917–3924 (1999)

Wang, X.P., Yu, J.J., Cheng, J., Hao, Z.P., Xu, Z.P.: High-temperature adsorption of carbon dioxide on mixed oxides derived hydrotalcite-like compounds. Environ. Sci. Technol. **42**, 614–618 (2008)

Yang, Q., Zhong, C., Chen, J.F.: Computational study of CO_2 storage in metal-organic frameworks. J. Phys. Chem. C **112**, 1562–1569 (2008)

Yufeng, H., Seaton, N.A.: Heats of adsorption and adsorption heterogeneity for methane, ethane and carbon dioxide. Langmuir **22**, 1150–1155 (2006)